

1 2

# Training Convolutional Neural Networks with the Forward-Forward algorithm

**Riccardo Scodellaro**<sup>1,\*</sup>, †**Ajinkya Kulkarni**<sup>1</sup>, †**Frauke Alves**<sup>1,2,3</sup>**Matthias Schröter**<sup>3,4,\*</sup>

RICCARDO.SCODELLARO@MPINAT.MPG.DE

AJINKYA.KULKARNI@MPINAT.MPG.DE

FALVES@GWDG.DE

MATTHIAS.SCHROETER@MPINAT.MPG.DE

<sup>1</sup> *Translational Molecular Imaging  
Max Planck Institute for Multidisciplinary Sciences  
Hermann-Rein-Straße 3, 37075 Göttingen, Germany.*

<sup>2</sup> *Department of Haematology and Medical Oncology  
University Medical Center Göttingen  
Robert-Koch-Straße 40, 37075 Göttingen, Germany*

<sup>3</sup> *Institute for Diagnostic and Interventional Radiology  
University Medical Center Göttingen  
Robert-Koch-Straße 40, 37075 Göttingen, Germany*

<sup>4</sup> *subject to approval, some other place in Göttingen, Germany*

**Editor:** XXX

## Abstract

The recent successes in analyzing images with deep neural networks are almost exclusively achieved with Convolutional Neural Networks (CNNs). The training of these CNNs, and in fact of all deep neural network architectures, uses the backpropagation algorithm where the output of the network is compared with the desired result and the difference is then used to tune the weights of the network towards the desired outcome. In a 2022 preprint, Geoffrey Hinton suggested an alternative way of training which passes the desired results together with the images at the input of the network. This so called Forward Forward (FF) algorithm has up to now only been used in fully connected networks. In this paper, we show how the FF paradigm can be extended to CNNs. Our FF-trained CNN, featuring a novel spatially-extended labeling technique, achieves a classification accuracy of 99.0% on the MNIST hand-written digits dataset. We show how different hyperparameters affect the performance of the proposed algorithm and compare the results with CNN trained with the standard backpropagation approach. Furthermore, we use Class Activation Maps to investigate which type of features are learnt by the FF algorithm.

**Keywords:** Forward-Forward, keyword two, keyword three

---

1. \* corresponding authors

2. † equal contribution

## 1 Introduction

Machine learning using deep neural networks (DNN) continues to transform human live in areas as different as art (DALL-E, stable diffusion), medicine (Alpha-Fold), transport (self-driving cars, any time now), or information retrieval (ChatGPT, Bard). Here, the adjective deep refers to the number of layers of artificial neurons which can go up to the hundreds. Training these networks means to shift the weights connecting the layers from their initial, random values to values which produce the correct predictions at the output layer of the DNN. This is achieved with the help of a loss function that computes the aggregate difference between the predicted output and the accurate results, which must be known for the training examples. The algorithm behind the training is some variant of gradient descent: in each round of training each weight is shifted a bit into the direction minimizing the loss by using the derivative of the loss function with respect to that weight.

Taking the derivative of a loss function with respect to a given weight is straightforward for a single, output layer. Training the weights of the earlier layers in DNN requires the gradient computation to be performed iteratively by applying the chain rule (Rumelhart et al., 1986). This process is called backpropagation (BP). Due to its importance, the term BP is also often used loosely to refer to the entire learning algorithm including the gradient descent.

Backpropagation, respectively multi-layer gradient descent, has a number of downsides: first, it requires the storage of intermediate results. Depending on the optimizer, the memory consumption of BP is up to 5 times larger than the requirement for storing the weights alone (Hugging Face Community, 2023). This becomes a problem when training large models on GPU cards with limited memory. Second, under the name neuromorphic computing there is an ongoing search of hardware alternatives to CMOS semiconductors, driven by the desire to decrease power consumption and increase processing speed (Christensen et al., 2022). On these new hardware platforms it is often impossible to implement an analog of BP, raising the need for alternative training algorithm. Finally, evolution has clearly developed learning algorithms for neural networks such as our brain. However, those algorithms seem to be quite (but maybe not completely (Lillicrap et al., 2020)) different from BP. Given the in general high performance of evolutionary solutions to problems, this raises the question if also deep learning could gain from biologically plausible alternatives to BP.

Due to this limitations, there is an ongoing search for alternative training methods. The most radical approach is to abandon the loss function completely and use a new learning paradigm. Neural networks trained with variants of the locally acting Hebbian learning rule (neurons that fire together wire together) have been shown to be competitive with BP (Journé et al., 2023; Zhou, 2022). Another approach, Equilibrium Propagation (Scellier and Bengio, 2017) is a learning framework for energy based models with symmetric connections between neurons. Layer-wise Feedback Propagation (Weber et al., 2023) removes the need for a gradient computation by replacing the objective of reducing the loss with computing a reward signal from the network output and propagating that signal backward into the net.

In contrast, the most conservative approach is to keep gradient descent, but to replace the required gradients with an estimate computed from the difference in loss of two forward passes with slightly modified weights. While the naive version of this approach, labeled zeroth order optimization, can be expected to be extremely inefficient, modern variants

seem to be competitive (Baydin et al., 2022; McCaughan et al., 2023; Malladi et al., 2023; Zhao et al., 2023b).

A third category of algorithms maintains the idea to update the weights using derivatives of some signal involving the difference between the present state of the network and the target state. But to relax the requirement to propagate that signal from the output layer backward towards the input. This can either be done by using exclusively an output-derived error signal for training each intermediate layer (Nøkland, 2016; Flügel et al., 2023), or by training each layer with locally available information gathered in two consecutive forward passes. An examples of the latter is the "Present the Error to Perturb the Input To modulate Activity technique" (PEPITA), which performs the second forward pass with the sum of the input signal used in the first pass and some random projection of the error signal from that pass (DellaFerrera and Kreiman, 2022; Farinha et al., 2023).

Another example of the use of local information gathered in consecutive runs to update the weights is the Forward-Forward (FF) algorithm proposed by Geoffrey Hinton in December 2022. FF training combines two ideas. First, the weights of a given layer are updated using gradients of a locally defined goodness function, which in the original paper is taken to be the sum of the squares of the activities in that layer. Second, the labels are included in the training data which allows the neurons to learn them together. In order to understand which features of the data 'vote' for a given label, half of the dataset is comprised of labels combined with wrong images. For this negative data the weights are changed in order to minimize the goodness. In contrast, for the correctly labeled, positive data the weights are modified to maximize the goodness. Both these objectives can be achieved with a local gradient descent, with no need for BP. The term Forward Forward now refers to having two subsequent training steps, one with positive and one with negative data.

When generalizing this training method to multi-layer networks, it is important to assure that each subsequent layer needs to do more than just measure the length of the activity vector of the previous one. This is achieved by using layer normalization (Ba et al., 2016) which normalizes the activity vector for each sample. This is best summarized by the description in Hinton (2022): *the activity vector in the first hidden layer has a length and an orientation. The length is used to define the goodness for that layer and only the orientation is passed to the next layer.*

There are two ways of using a FF trained network for inference. First, we can simultaneously train a linear classifier using the activities of the neurons in the different layers as input. Alternatively, we can create multiple copies of the dataset under consideration and combine each copy with one of the possible labels. The correct label is then the one with the largest goodness during its forward pass. Note that this approach multiplies the amount of computation required for inference with a factor equal to the number of labels.

Given the repute of the proposer, it is not surprising that the Forward Forward algorithm has inspired a number of groups to suggest modified and adapted versions. Examples include the combination with a generative model (Ororbia and Mali, 2023), multiple Convolutional Blocks (not trained with FF) (Zhao et al., 2023a), or extending FF training to Graph Neural Networks (Paliotta et al., 2023) and Spiking Neural Networks (Ororbia, 2023). In accordance with the neuromorphic computation motivation of moving beyond BP, the FF algorithm has also been used to train optical neural networks (Oguz et al., 2023) and microcontroller units with low computational resources (De Vita et al., 2023). Another line

of research tries to improve FF by modifications how the goodness is computed (Lee and Song, 2023; Lorberbom et al., 2023; Gandhi et al., 2023), by understanding the sparsity of activation in FF trained networks (Tosato et al., 2023; Yang, 2023), or by exploring the capabilities of FF for self-supervised learning (Brenig and Timofte, 2023).

There has been less activity in terms of practical applications of the FF algorithm. Particularly, in the classification of real world images it has been noted that FF performs worse than BP (Reyes-Angulo and Paheding, 2023) or has to be combined with BP to achieve satisfying results (Paheding and Reyes-Angulo, 2023). We propose that this lack of applications is due to the absence of a method to train the mainstay of modern image processing, Convolutional Neural Networks (CNN) (Rawat and Wang, 2017), with the FF algorithm. The ideas presented here close this gap.

Firstly, we showed how we developed our FF-trained CNN. We described the implementation of a spatial-extended labeling, crucial to preserve the label information in the image during convolution, and the mathematical steps underneath both the FF-based learning algorithm and the inference approaches proposed by Hinton (2022). Then, we showed the results of the tests performed with our first FF-trained CNN architecture on the hand-written digits of the MNIST dataset: we obtained a classification accuracy of 99.14% for the validation set and 99.00% for the test dataset, comparable to the results of conventional backpropagation-based networks. Furthermore, we characterized the novel developed CNN by evaluating how its hyperparameters affect the network performances. Finally, we provided the results of a preliminary investigation, conducted by exploiting Class Activation Maps (CAMs), aimed to evaluate which image-based features are processed by the FF paradigm to accomplish classification task.

## 2 Materials and Methods

### 2.1 Spatially-extended labelling

Fully connected DNN establish connections between each pixel within an image and with each neuron in the next layer. The size of images is often of the order of mega pixels and typical layers have hundreds of neurons. This results in a number of weights to be trained which far exceeds the information available in typical training datasets. In contrast, convolutional layers use small filter kernels, typically sized in the range of 3 by 3 to 7 by 7 pixels, which are applied to all possible positions of the much larger input picture. In this way, each filter creates a new, processed version of the input image. Because the training algorithm only needs to learn the weights in these filter kernels, it is possible to apply hundreds of these kernels in parallel and still have order of magnitudes less parameters to train than in a fully connected network.

FF training requires the labels to be added to the input images. Hinton (2022) achieves this with an one-hot encoding in which the label information is confined to the first 10 pixels in the upper left region of each image. **Figure 1 A** and **B** give an example of this technique. However, convolutional layers will not work with this one-hot encoding because for most of the possible positions of the filter kernel, these labels are not part of the input. For CNN it is imperative for the label information to be spatially present over the entire image, ensuring that it is captured by each possible filter position. Moreover, this spatial

labeling needs to be homogeneous; concatenated random patterns, as used by Lee and Song (2023), will also not allow for arbitrary filter positions.

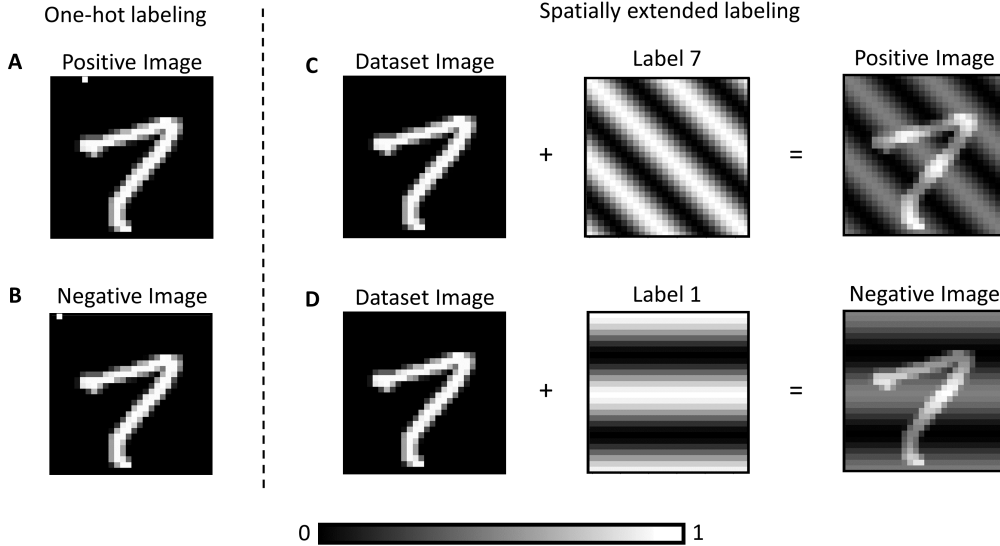


Figure 1: **Spatially-extended labels are present in the entire image, while one-hot encoding is confined in the upper-left area.** For the FF training we need two datasets which both add labels to the images. The top row describes the creation of the positive dataset, where the example image is correctly labeled as seven. The bottom row displays an example of the negative dataset where the image is combined with a false label (here a one) which was randomly chosen from the 9 possible ones. Left and right of the dashed line we display the two ways of adding the label. Panels A and B describe the one-hot encoding used in Hinton (2022): the first ten pixels in the top row of the image, which are usually black/zero, are used as indicators. The column number of the single pixels set to 1 corresponds to the target value. Panels C and D describe the technique used by us in this paper. Each label corresponds to an image of the same size as the input, but with a characteristic gray value wave. The label is included into the image by pixel-wise addition.

Here, we introduce a spatial-extended labeling approach involving the superposition of the training dataset image with a second image of identical dimensions. This additional image consists of a gray-value wave with a fixed frequency, phase, and orientation. Each possible label is associated with a distinct configuration of these three parameters.

As indicated in **Figure 1 C and D**, both the positive and negative datasets are obtained by harnessing this methodology. Labels are created by starting from an empty 2D Fourier space of the same size than the image. We then set a single 2D Fourier mode to a finite amplitude  $i$ . The mapping between the labels and the wavelength and orientation of the corresponding mode is a matter of choice; we have tested two different options. Set 1, which is reported in **Figure 2**, is characterized by a combination of 4 different wave

orientations ( $0^\circ$ ,  $45^\circ$ ,  $90^\circ$ ,  $135^\circ$ ) and three different frequencies. Set 2, as shown in **Figure 7** in the appendix, uses only one spatial frequency and obtains the different labels from ten equidistant angular orientations in the range  $[0^\circ, 180^\circ]$ . After the superposition of the label, the images are again normalized to the range 0 to 1. The relative contribution  $K$  of the label pattern to the total intensity of the image is a hyperparameter whose influence will be described in section 3.2.3. Note that we choose our negative labels randomly, not specifically hard based on another forward pass, as it was done in Hinton (2022).

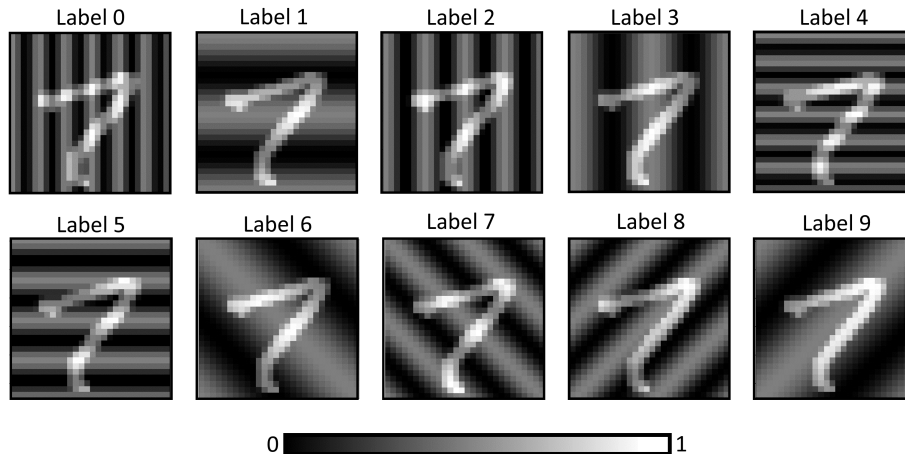


Figure 2: **Superposition of an image of the digit 7 with the full first set of waves used for the spatially-extended labelling.** Only the image with the label 7 is part of the positive dataset, while one of the other nine images is randomly selected to be part of the negative dataset.

## 2.2 Implementation of the learning algorithm

The present study uses a network architecture composed of three consecutive FF-trained convolutional layers. All three layers contain the same number of filter matrices which is one of the hyperparameter we examined. We did not add any max pooling layers because we found that those decrease accuracy as described in section C in the appendix. All neurons use ReLU as activation function.

All results reported are obtained using the MNIST handwritten digits dataset (LeCun and Cortes (2010)). We split the original training data into 50,000 images used for training and 10,000 validation images used in the search for the optimal hyperparameters. The original 10,000 test images were only used for obtaining the final result reported in section 3.1. All reported accuracies are averaged over 5 independent runs.

Just as in the FF training of DNN, we evaluate the loss of each convolutional layer by computing the sigmoidal function  $\sigma$  of the goodness. The goodness is defined as the sum of squared layer activations  $y_i$ , modified by subtracting a user-provided threshold  $\theta$ . Following

the code provided by Geoffrey Hinton<sup>1</sup>, and as confirmed by Gandhi et al. (2023), we choose  $\theta$  to be equal to the number of neurons  $N$  within that layer.

While computing the loss, we have to account for our different objectives regarding positive and negative data:

$$\text{loss}_{\text{layer}} = \sigma \left( \sum_{i=1}^N \begin{cases} y_i^2 - \theta & \text{if positive data} \\ -y_i^2 + \theta & \text{if negative data} \end{cases} \right) \quad (1)$$

We do not induce symmetry in our loss as described in Lee and Song (2023). But we took inspiration from Lorberbom et al. (2023) who found improved collaboration between layers by training them with a cumulative network loss, computed by summing the individual layer losses  $\text{loss}_{\text{layer}}$ . Here, we exclude the loss of the first layer since it yielded better accuracy as shown in **Section B** in the appendix. This also aligns with Hinton’s exclusion of the first layer during the evaluation phase.

We follow the implementation of Hinton (2022) in two more aspects. First, we apply layer normalization between the individual layers. As described in Ba et al. (2016), layer normalization involves the application of the following transformation to each activation  $y_i$ :

$$y_{i,\text{norm}} = y_i / \left( \sqrt{\frac{\sum_{i=1}^N y_i^2}{N}} \right) \quad (2)$$

This assures that each subsequent layer can only use the pattern not the norm of the matrix formed by the activations of the previous layer. Second, the learning rate is modified halfway through the epochs by employing a linear cooldown:

$$lr_e = \frac{2}{E} lr (1 + E - e) \quad (3)$$

where  $E$  represents the total number of epochs and  $e$  is the current epoch.

In order to study the contribution of the individual layers we define a layer based loss and accuracy which measure only the capability to discriminate between images of the positive and negative dataset. We interpret the output of the sigmoid function as a probability, where values  $> 0.5$  indicate that the layer recognizes the image as belonging to the positive dataset. By comparing the true assignment (positive or negative) we obtain a discrimination accuracy. And by using the probability to compute a binary cross entropy, we compute a layer-specific discrimination loss.

### 2.3 Two ways of inference

There are two ways how an FF trained CNN or DNN can be used for inference: the linear classifier and the goodness evaluation. In the first case, the  $H$  neurons of every layer except the first are fully-connected with an output layer of  $N$  nodes, equal to the number of labels. The connecting weights,  $H$  times  $N$  in number, are trained by evaluating the neuron activations using a cross-entropy loss.

---

1. The webpage of Prof. Hinton includes a demonstration code at <https://www.cs.toronto.edu/~hinton/>.

For inference with goodness evaluation, each image is exposed  $N$  times to the neural network, each time superimposed with another of the  $N$  possible labels. The goodness parameter is computed for each label and the image is associated with the label characterized by the highest goodness value:

$$\text{label}_{\text{correct}} = \operatorname{argmax} \left( \begin{bmatrix} f_0 \\ f_1 \\ \vdots \\ f_9 \end{bmatrix} \right) \quad (4)$$

where goodness is expressed as  $f_m = \sum_{i=1}^H y_i^2$  for each associated label  $m$  and  $H$  is again the number of all neurons, except those from the first layer.

## 2.4 Hardware and Software

The code for our FF trained CNN is implemented in Python using the PyTorch library. We took the code of Loewe (2023) for an FF trained, fully connected DNN as the starting point for our own efforts. Our code is available on a GitHub <sup>2</sup>. All analysis presented here was performed on a desktop workstation with an AMD Ryzen 9 5900X 12-Core Processor and 125 GB RAM.

## 3 Results

We first report the configuration which achieved the highest accuracy, then the search through the space of hyperparameters (using only our validation dataset) leading to that optimal configuration. We close by demonstrating the ability of FF trained CNN to implement Class Activation Maps, which is a method from the explainable AI toolbox.

### 3.1 Performance of optimized configuration

The hyperparameters optimization lead to the following configuration for the FF trained CNN: three convolution layers of each 128 filters with a kernel dimension of 7x7 pixels. Even though the goodness computation provides a better accuracy, the inference is performed for time reasons with the linear classifier approach. After training for 200 epochs with a batch size of 50, ADAM optimizer with learning rate =  $5 \times 10^{-5}$ , and the label set 1 (**Figure 2**) with intensity  $K = 35\%$  we obtained 99.14% accuracy for the validation dataset and 99.00% for the test dataset (the latter is presently averaged only over 2 runs).

For comparison, using again a three layer CNN of constant size but trained with BP with obtained a validation accuracy of 99.13% (16 filters of 5x5 pixels, Adam optimizer with learning rate =  $10^{-3}$ , 200 epochs, batch size = 50).

**Figure 3** provides a more detailed picture of this comparison. **Figure 3 A** show that the performance of FF training increases monotonously with the number of filters while BP training accuracy decreases slightly under the same conditions. The latter is most likely an effect due to increasing overfitting; its absence indicates that FF training might either be

---

2. code will be available after publication in peer-reviewed journal

more robust against overfitting, or that it makes less efficient use of its number of trainable parameters.

The confusion matrix (**Figure 3 B**) provides insights into the classification performance, revealing that labels 5 and 9 exhibit the least accurate classifications (lower than 98.20%), while labels 6, 7 and 1 are characterized by the highest accuracy levels (higher than 99.50%).

After 200 epochs, discrimination loss of the FF trained network reaches a plateau for all considered layers (**Figure 3 C**). This was confirmed by a training with 750 epochs which resulted in no substantial changes in accuracy. Moreover, the network exhibited convergence, as evidenced not only by the overall accuracy value on the training data reaching close to 100% (as depicted in **Figure 3 D** with a green line), but also by the discrimination accuracy values achieved by each layer (red and blue lines), which both independently recognized the images of the positive and the negative datasets.

In order to investigate the effect of the goodness of the first convolutional layer, we trained the CNN which reached the best accuracy value for a second time while adding also the goodness value computed from the first layer to the total goodness. **Figure 8** in the appendix reports the results, highlighting that the training of the first layer affects the fast convergence of the next layer and reduces the overall accuracy of the network by approximately 2%.

### 3.2 FF-trained CNN hyperparameters characterization

The best FF-trained CNN architecture we proposed has been obtained by characterizing different parameters, which can affect the network classification performance. These analysis were performed by using a constant learning rate of  $5 \times 10^{-5}$ , which was empirically found to be optimal for the FF-trained network in the wide range between  $10^{-2}$  and  $10^{-7}$ , over 200 epochs. Initially, we refrained from incorporating supplementary layers such as fully-connected, dropout, or pooling layers. Indeed, only in the final phase of our investigation we introduced max pooling layers to assess their impact. This choice was motivated by our intention to underscore the autonomous capability of the novel FF-trained CNN in effectively processing information gleaned from dataset images, thus aptly executing classification tasks. Moreover, no competitive results were achieved by applying max pooling layers, as more extensively described by 2

#### 3.2.1 FILTER DIMENSIONS AND BATCH SIZE

Firstly, we focused on assessing critical hyperparameters that define the FF-trained CNN, including filter dimensions used during convolution, network complexity represented by the number of filters per layer, and the exploited batch size. **Figure 4 B** shows that more complex FF-trained architectures and 7x7 pixel filters demonstrated superior accuracy. Specifically, the 128x128x128 architecture consistently delivered the highest accuracy across all tested filter dimensions (3x3, 5x5, 7x7). Moreover, the 7x7 filter configuration yielded the best results irrespective of the number of filters employed. The 64x64x64 configuration also provided reliable results, although it slightly trailed the top-performing setup tested (128x128x128 filters of 7x7 pixel dimensions). As shown in **Figure 4 A**, for 5x5 and 7x7 filters better results were achieved for lower batch sizes, while the computational time needed for the training phase increased considerably. Specifically,  $43.1 \pm 0.8\%$  s/epoch

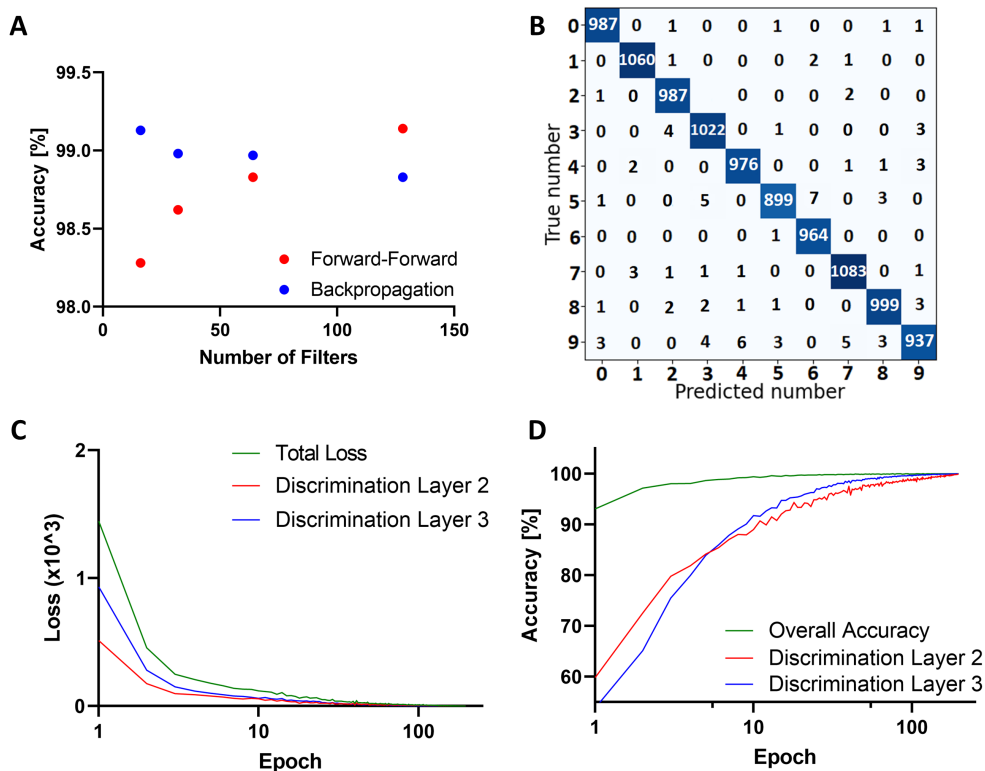


Figure 3: **Best performance of FF-trained CNN architecture on MNIST dataset is comparable to the backpropagation-based architectures outcome.** The best configuration we obtained for the FF-trained CNN reached 99.14% of accuracy and was characterized by 128 filters of 7x7 pixels for each layer, Adam optimizer, epochs = 200, batch size = 50, learning rate =  $5 \times 10^{-5}$ , varying frequencies (set 1) labeling with  $K = 35\%$ . (A) shows the accuracy values obtained for both FF and backpropagation-trained (learning rates of  $5 \times 10^{-5}$  and  $10^{-3}$ , respectively) CNNs of three convolutional layers by varying the number of filters per layer (16, 32, 64, 128) and fixing epochs = 200 and batch size = 15. (B) reports the confusion matrix describing the classification performance of the FF-trained CNN on the validation dataset for its best configuration. (C) shows the loss values concerning the discrimination between positive and negative training data for each considered hidden layer (red and blue lines), and the loss value related to the training data digits classification (green line) (D) shows the accuracy values concerning the discrimination between positive and negative training data for each considered hidden layer (red and blue lines), and the accuracy value obtained by the network architecture on the training data concerning their digits classification (green line).

were necessary to train the 64x64x64 network with batch sizes of 25 elements. Conversely, employing a batch size of 50 elements under the same configuration reduced the required training time to  $21.9 \pm 0.3\%$  s/epoch.

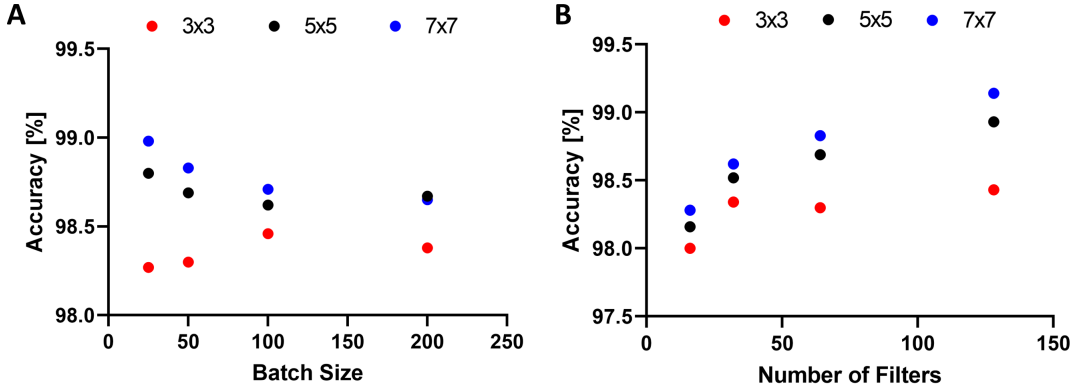


Figure 4: **The top-performing setup of a FF-trained CNN is characterized by a small batch size and a complex architecture, which employs a high number of filters** (A) Accuracy values obtained by varying the batch size (25, 50, 100, 200) and the filter dimension (3x3, 5x5, 7x7 pixels) in a network of three convolutional layers of 64x64x64 filters. Network parameters: learning rate =  $5 \times 10^{-5}$ , epochs = 200, Adam optimizer. (B) Accuracy values obtained by varying the number of filters per layer (16, 32, 64, 128) and the filter dimensions (3x3, 5x5, 7x7 pixels) in a network of three convolutional layers. Network parameters: batch size = 50, learning rate =  $5 \times 10^{-5}$ , epochs = 200 with the Adam optimizer.

### 3.2.2 LINEAR CLASSIFIER VS. GOODNESS APPROACH

Another aspect to investigate pertains to the inference approach. We assessed both the linear classifier and the goodness computation methods for different CNNs, as outlined in **Table 1**. Each method is associated with an optimal learning rate of  $5 \times 10^{-5}$ . As shown also by Brenig and Timofte (2023), the goodness approach yielded slightly superior results, although the computational time was longer both during the training and during the validation phases. This discrepancy arises because, in the goodness method, each image in the dataset must be processed for each label in order to perform the classification task. The goodness accuracy computation proves to be valuable for datasets with a small number of labels. However, for datasets with a larger number of labels, the marginal improvements offered by this method may not be justified. Goodness can be employed in scenarios where the computational time is not a critical factor. Since preserving computing resources is a primary objective of the FF algorithm, the linear classifier is the preferred choice. Consequently, we proceeded to evaluate the best configuration by exclusively using this approach.

FF-CNN Network	Linear Classifier		Goodness	
	Accuracy [%]	Time/epoch [s]	Accuracy [%]	Time/epoch [s]
128x128x128, batch=50, filter 5x5	98.93	43.1 ± 0.6 s	99.04	331 ± 13 s
16x16x16, batch=50, filter 5x5	98.16	7.6±0.2 s	98.75	154 ± 1 s
64x64x64, batch=50, filter 3x3	98.30	21.9±0.3 s	98.82	288 ± 6 s
64x64x64, batch=200, filter 5x5	98.67	7.6±0.2 s	98.94	150 ± 1 s

Table 1: **The goodness approach demonstrates better performance compared to the linear classifier, albeit at higher computational cost.** Four FF-trained CNNs were trained by using the set 1 labeling, the Adam optimizer and 200 epochs. The classification was performed by applying the linear classifier or the goodness computation (learning rate of  $5 \times 10^{-5}$ ). The uncertainties on the accuracy and time per epoch values were obtained by computing the standard deviation on the results of 5 different repetitions. Accuracy values are characterized by an uncertainty of  $\pm 0.01$ .

### 3.2.3 EFFECT OF THE RELATIVE LABELING INTENSITY $K$

We explored the impact on the network performance of varying relative intensity contributions of the labeling pattern on both positive and negative datasets. We focused on architectures that exhibited the highest accuracy values: 128x128x128 and 64x64x64 filters. We tested batch sizes of 25 and 50 elements. Each architecture featured 7x7 pixel filters, a learning rate of  $5 \times 10^{-5}$ , 200 epochs, and employed the Adam optimizer. Comprehensive results were presented in **Figure 5**. Optimizing label intensity led to an increase in networks accuracy by up to 0.2%. Specifically, the tested 64x64x64 architectures exhibited their highest accuracy values when the label intensity contribution  $K$  was set  $\approx 65\%$ . In contrast, the 128x128x128 networks attained their peak result with a label relative intensity of  $K \approx 35\%$ , irrespective on the elected batch size. This leads to the conclusion that the optimal value of labeling intensity, represented by  $K$ , should be determined based on the specific network architecture. Conversely, when internal parameters, such as filter dimensions and batch size, are modified, there is no need to re-optimize the value of  $K$ .

### 3.3 Class Activation Maps for explainable AI applications

Class Activation Maps (CAMs) are visual representations that highlight the regions of an input image which provide maximum information to distinguish a specific label. CAMs are obtained by summing the feature maps generated by the convolutional layers, which encode specific spatial characteristics of the image, weighted by their corresponding weights associated with a specific label. These weights quantify how much each considered spatial feature contributes to the recognition of the target class. This technique helps in understanding and interpreting the network behavior in image analysis.

In this context, we exploited each activation value within the hidden convolutional layers used for the classification task. These activations were multiplied by their corresponding weights linked to the image label and obtained from the linear classifier. This architecture enabled the generation of CAMs characterizing the images of the validation dataset. Four examples were reported in **Figure 6**, obtained by exploiting a 16x16x16 FF-trained CNN

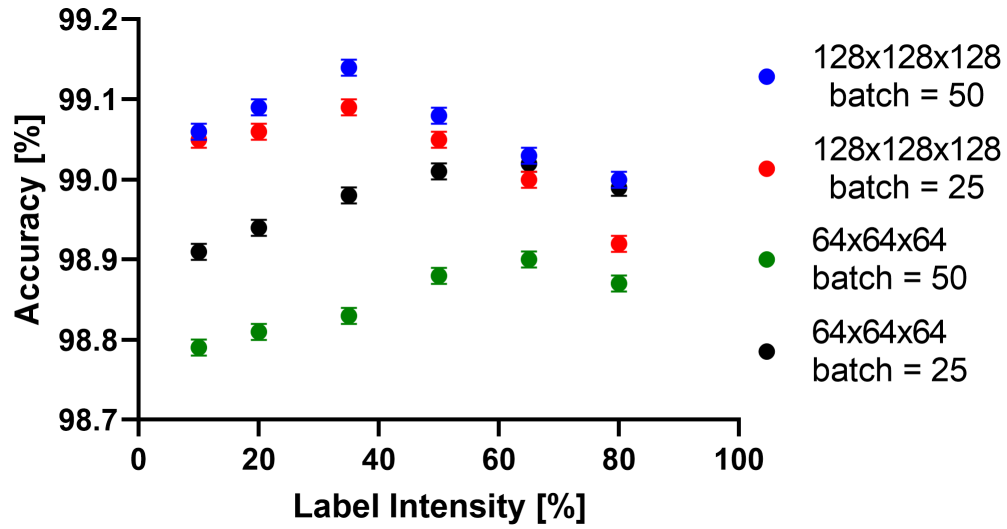


Figure 5: **The best choice of the relative label intensity  $K$  is dependent on the FF-trained CNN architecture.** Accuracy values obtained by varying the relative intensity contribution of the labeling pattern  $K$  on the positive and negative datasets. The analysis was conducted for four FF-CNN network architectures: 128x128x128 filters with batch size = 50 and 25, 64x64x64 filters with batch size = 50 and 25. Networks parameters: filters dimension of 7x7, learning rate =  $5 \times 10^{-5}$ , epochs = 200, Adam optimizer.

architecture, characterized by filters of 5x5 pixels, Adam optimizer, epochs = 200, batch size = 50, learning rate =  $5 \times 10^{-5}$  and varying frequencies (set 1) labeling. The CAMs highlighted which spatial information were processed by the FF-trained CNNs to provide correct classifications. The entire vertical shape was considered to recognize the number 1 (**Figure 6 A-B**), while three different areas (the upper, the bottom-left and the bottom right parts of the number) were exploited to classify the number 2 (**Figure 6 5C-D**). The number 7 were recognized basing almost only on its long horizontal line, correlated with the ends of its vertical line (**Figures 6 E-F**). A digit were classified as a 9 by considering the presence of a round-shape figure, characterized by an appendix in its bottom region.

CAMs also showed that each layer of the FF-trained CNN provides distinct and valuable information for the classification task. This is demonstrated by visualizing the regions independently exploited by each layer of the network to accomplish the classification task (**Figure 9, Appendix A**). For instance, when considering the digit 7, the second layer of the network provides the most valuable information concerning the inner portion of the horizontal line characterizing the number 7, while the third layer offers more information about the boundaries of the horizontal line.

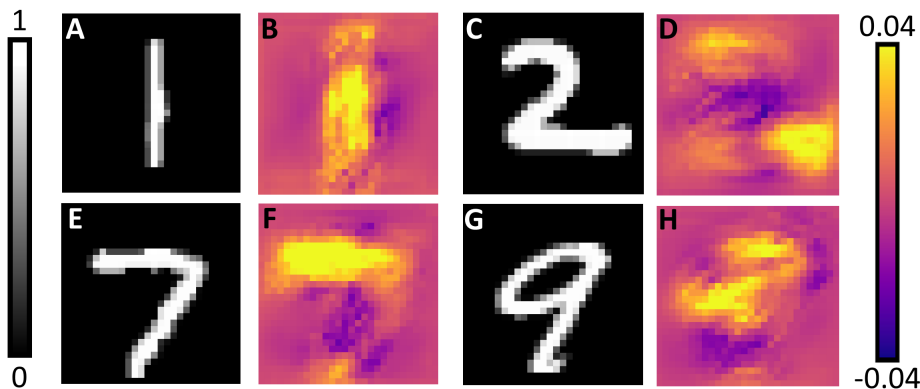


Figure 6: **CAMs of FF-trained CNN show which image regions are considered by the network for successful classification task** (A) Image from the validation dataset depicting the number one, correctly classified. (B) Corresponding CAM for (A), referred to its correct labeling. (C) Validation dataset image showing the number two, correctly classified. (D) CAM for (C), associated with its correct labeling. (E) Validation dataset image representing a number seven, correctly classified. (F) Class Activation Map of (E), referred to its correct labeling. (G) Validation dataset image representing a number two, correctly classified by the network. (H) CAM for (G), connected to its correct labeling.

#### 4 Discussion and Conclusions

CNNs are considered the gold standard in deep learning-based image analysis. For instance, in biomedical imaging they overcome the drawbacks of subjective analysis in the

semi-quantitative visual inspection of samples (Gurcan et al., 2009) and they support experts during their daily clinical routine by reducing their workload (Shmatko et al., 2022). Furthermore, their exploitation of the spatial information within images makes them suitable for the deployment of explainable AI tools (such as Class Activation Maps) which highlight the image regions contributing most significantly to the classification outcome.

Our implementation of FF trained CNN shows that with the right choice of hyperparameters this technique is competitive with backpropagation. These results were obtained without implementing all the possible and suggested optimizations such as enforcing symmetry of the loss function (Lee and Song, 2023) or choosing hard, i.e. easily confused, labels for the negative dataset as suggested by Hinton (2022). We propose that our work shows the potential of FF trained CNNs to address real world computer vision problems. If this technique will in some applications supersede BP is an open question. We believe that this potential exists, especially in the cases of neuromorphic hardware and unsupervised learning.

A better understanding of the FF training will however also expand our understanding of the generic concept of neuronal information processing in all its breadth from biological systems to reservoir computing. The here demonstrated capability of implementing Class Activation Maps provides a first window into these research topics. Achieving deeper insights will also mean to understand how the two innovations of FF, providing positive and negative labels and computing a locally defined goodness parameter, contribute to its success individually and synergetically (Tosato et al., 2023).

Subsequent work on FF training should also address its ability to train deeper networks, most likely expanding on the work of Lorberbom et al. (2023). Also the ability of FF training to work with larger and more complex datasets needs to be explored. Finally, its connection to biological neuronal systems (Ororbia and Mali, 2023; Ororbia, 2023) seems a promising research direction.

## Acknowledgments and Disclosure of Funding

This project has received funding from the Innovative Medicines Initiative 2 Joint Undertaking (JU) under grant agreement No 101034427. The JU receives support from the European Union’s Horizon 2020 research and innovation program and EFPIA. The JU is not participating as a contracting authority in this procurement. This project was also funded by the Ministry for Science and Culture of Lower Saxony as part of the project “Agile, bio-inspired architectures” (ABA).

## References

- Jimmy Lei Ba, Jamie Ryan Kiros, and Geoffrey E. Hinton. Layer normalization. *arXiv*. 1607.06450, 2016.
- Atılım Güneş Baydin, Barak A. Pearlmutter, Don Syme, Frank Wood, and Philip Torr. Gradients without backpropagation. *arXiv:2202.08587*, 2022.

- Jonas Brenig and Radu Timofte. A study of forward-forward algorithm for self-supervised learning. [arXiv:2309.11955](#), 2023.
- Dennis V. Christensen, Regina Dittmann, Bernabe Linares-Barranco, Abu Sebastian, Manuel Le Gallo, Andrea Redaelli, Stefan Slesazek, Thomas Mikolajick, Sabina Spiga, Stephan Menzel, Ilia Valov, Gianluca Milano, Carlo Ricciardi, Shi-Jun Liang, Feng Miao, Mario Lanza, Tyler J. Quill, Scott T. Keene, Alberto Salleo, Julie Grollier, Danijela Marković, Alice Mizrahi, Peng Yao, J. Joshua Yang, Giacomo Indiveri, John Paul Strachan, Suman Datta, Elisa Vianello, Alexandre Valentian, Johannes Feldmann, Xuan Li, Wolfram H. P. Pernice, Harish Bhaskaran, Steve Furber, Emre Neftci, Franz Scherr, Wolfgang Maass, Srikanth Ramaswamy, Jonathan Tapson, Priyadarshini Panda, Youngeun Kim, Gouhei Tanaka, Simon Thorpe, Chiara Bartolozzi, Thomas A. Cleland, Christoph Posch, ShihChii Liu, Gabriella Panuccio, Mufti Mahmud, Arnab Neelim Mazumder, Morteza Hosseini, Tinoosh Mohsenin, Elisa Donati, Silvia Tolu, Roberto Galeazzi, Martin Ejsing Christensen, Sune Holm, Daniele Ielmini, and N. Pryds. 2022 roadmap on neuromorphic computing and engineering. *Neuromorphic Computing and Engineering*, 2:022501, 2022. doi: 10.1088/2634-4386/ac4a83.
- Fabrizio De Vita, Rawan M. A. Nawaiseh, Dario Bruneo, Valeria Tomaselli, Marco Latuada, and Mirko Falchetto.  $\mu$ -FF: On-Device Forward-Forward Training Algorithm for Microcontrollers. In *2023 IEEE International Conference on Smart Computing (SMARTCOMP)*, pages 49–56, 2023. doi: 10.1109/SMARTCOMP58114.2023.00024.
- Giorgia Dellaferrera and Gabriel Kreiman. Error-driven input modulation: Solving the credit assignment problem without a backward pass. In *Proceedings of the 39th International Conference on Machine Learning*, Proceedings of Machine Learning Research, pages 4937–4955, 2022.
- Matilde Tristany Farinha, Thomas Ortner, Giorgia Dellaferrera, Benjamin Grewe, and Angeliki Pantazi. Efficient biologically plausible adversarial training. [arXiv:2309.17348](#), 2023.
- Katharina Flügel, Daniel Coquelin, Marie Weiel, Charlotte Debus, Achim Streit, and Markus Götz. Feed-forward optimization with delayed feedback for neural networks. [arXiv:2304.13372](#), 2023.
- Saumya Gandhi, Ritu Gala, Jonah Kornberg, and Advaith Sridhar. Extending the forward forward algorithm. [arXiv:2307.04205](#), 2023.
- Metin N. Gurcan, Laura E. Boucheron, Ali Can, Anant Madabhushi, Nasir M. Rajpoot, and Bulent Yener. Histopathological image analysis: A review. *IEEE Reviews in Biomedical Engineering*, 2:147–171, 2009. doi: 10.1109/RBME.2009.2034865.
- Geoffrey Hinton. The forward-forward algorithm: Some preliminary investigations. [arXiv:2212.13345](#), 2022.
- The Hugging Face Community. Anatomy of model’s memory, 2023. URL [https://huggingface.co/docs/transformers/v4.36.0/model\\_memory\\_anatomy#anatomy-of-models-memory](https://huggingface.co/docs/transformers/v4.36.0/model_memory_anatomy#anatomy-of-models-memory).

- Adrien Journé, Hector Garcia Rodriguez, Qinghai Guo, and Timoleon Moraitis. Hebbian deep learning without feedback. [arXiv:2209.11883](https://arxiv.org/abs/2209.11883), 2023.
- Yann LeCun and Corinna Cortes. MNIST handwritten digit database, 2010. URL <http://yann.lecun.com/exdb/mnist/>.
- Heung-Chang Lee and Jeonggeun Song. Symba: Symmetric backpropagation-free contrastive learning with forward-forward algorithm for optimizing convergence. [arXiv:2303.08418](https://arxiv.org/abs/2303.08418), 2023.
- Timothy P. Lillicrap, Adam Santoro, Luke Marris, Colin J. Akerman, and Geoffrey Hinton. Backpropagation and the brain. *Nature Reviews Neuroscience*, 21(6):335–346, 2020. doi: 10.1038/s41583-020-0277-3.
- Sindy Loewe. The Forward-Forward Fully-Connected Network Implementation, 2023. URL <https://github.com/loeweX/Forward-Forward>.
- Guy Lorberbom, Itai Gat, Yossi Adi, Alex Schwing, and Tamir Hazan. Layer collaboration in the forward-forward algorithm. [arXiv:2305.12393](https://arxiv.org/abs/2305.12393), 2023.
- Sadhika Malladi, Tianyu Gao, Eshaan Nichani, Alex Damian, Jason D. Lee, Danqi Chen, and Sanjeev Arora. Fine-tuning language models with just forward passes. [arXiv:2305.17333](https://arxiv.org/abs/2305.17333), 2023.
- Adam N. McCaughan, Bakhrom G. Oripov, Natesh Ganesh, Sae Woo Nam, Andrew Diestfrey, and Sonia M. Buckley. Multiplexed gradient descent: Fast online training of modern datasets on hardware neural networks without backpropagation. *APL Machine Learning*, 1, 2023. doi: 10.1063/5.0157645.
- Arild Nøkland. Direct Feedback Alignment Provides Learning in Deep Neural Networks. In D. Lee, M. Sugiyama, U. Luxburg, I. Guyon, and R. Garnett, editors, *Advances in Neural Information Processing Systems*, volume 29. Curran Associates, Inc., 2016.
- Ilker Oguz, Junjie Ke, Qifei Weng, Feng Yang, Mustafa Yildirim, Niyazi Ulas Dinc, Jih-Liang Hsieh, Christophe Moser, and Demetri Psaltis. Forward–forward training of an optical neural network. *Opt. Lett.*, 48(20):5249–5252, 2023. doi: 10.1364/OL.496884.
- Alexander Ororbia. Contrastive-signal-dependent plasticity: Forward-forward learning of spiking neural systems. [arXiv:2303.18187](https://arxiv.org/abs/2303.18187), 2023.
- Alexander Ororbia and Ankur Mali. The predictive forward-forward algorithm. [arXiv:2301.01452](https://arxiv.org/abs/2301.01452), 2023.
- Sidike Paheding and Abel A. Reyes-Angulo. Forward-forward algorithm for hyperspectral image classification: A preliminary study. [arXiv:2307.00231](https://arxiv.org/abs/2307.00231), 2023.
- Daniele Paliotta, Mathieu Alain, Bálint Máté, and François Fleuret. Graph neural networks go forward-forward. [arXiv:2302.05282](https://arxiv.org/abs/2302.05282), 2023.

Waseem Rawat and Zenghui Wang. Deep Convolutional Neural Networks for Image Classification: A Comprehensive Review. *Neural Computation*, 29(9):2352–2449, 2017. doi: 10.1162/neco\_a\_00990.

Abel Reyes-Angulo and Sidike Paheding. The forward-forward algorithm as a feature extractor for skin lesion classification: A preliminary study. [arXiv:2307.00617](https://arxiv.org/abs/2307.00617), 2023.

David E. Rumelhart, Geoffrey E. Hinton, and Ronald J. Williams. Learning representations by back-propagating errors. *Nature*, 323(6088):533–536, 1986.

Benjamin Scellier and Yoshua Bengio. Equilibrium Propagation: Bridging the Gap between Energy-Based Models and Backpropagation. *Frontiers in Computational Neuroscience*, 11, 2017. doi: <https://doi.org/10.3389/fncom.2017.00024>.

Artem Shmatko, Narmin Ghaffari Laleh, Moritz Gerstung, and Jakob Nikolas Kather. Artificial intelligence in histopathology: enhancing cancer research and clinical oncology. *Nature Cancer*, 3(9):1026–1038, 2022. doi: 10.1038/s43018-022-00436-4.

Niccolò Tosato, Lorenzo Basile, Emanuele Ballarin, Giuseppe de Alteriis, Alberto Cazzaniga, and Alessio Ansuini. Emergent representations in networks trained with the forward-forward algorithm. [arXiv:2305.18353](https://arxiv.org/abs/2305.18353), 2023.

Leander Weber, Jim Berend, Alexander Binder, Thomas Wiegand, Wojciech Samek, and Sebastian Lapuschkin. Layer-wise feedback propagation. [arXiv:2308.12053](https://arxiv.org/abs/2308.12053), 2023.

Yukun Yang. A theory for the sparsity emerged in the forward forward algorithm. [arXiv:2311.05667](https://arxiv.org/abs/2311.05667), 2023.

Gongpei Zhao, Tao Wang, Yidong Li, Yi Jin, Congyan Lang, and Haibin Ling. The cascaded forward algorithm for neural network training. [arXiv:2303.09728](https://arxiv.org/abs/2303.09728), 2023a.

Yequan Zhao, Xinling Yu, Zhixiong Chen, Ziyue Liu, Sijia Liu, and Zheng Zhang. Tensor-compressed back-propagation-free training for (physics-informed) neural networks. [arXiv:2308.09858](https://arxiv.org/abs/2308.09858), 2023b.

Hongchao Zhou. Activation learning by local competitions. [arXiv:2209.13400](https://arxiv.org/abs/2209.13400), 2022.

## Appendix A. A second way of encoding the labels

For further information, refer to **Figure 7**.

## Appendix B. Contribution of the first layer

For further information, refer to **Figure 8**.

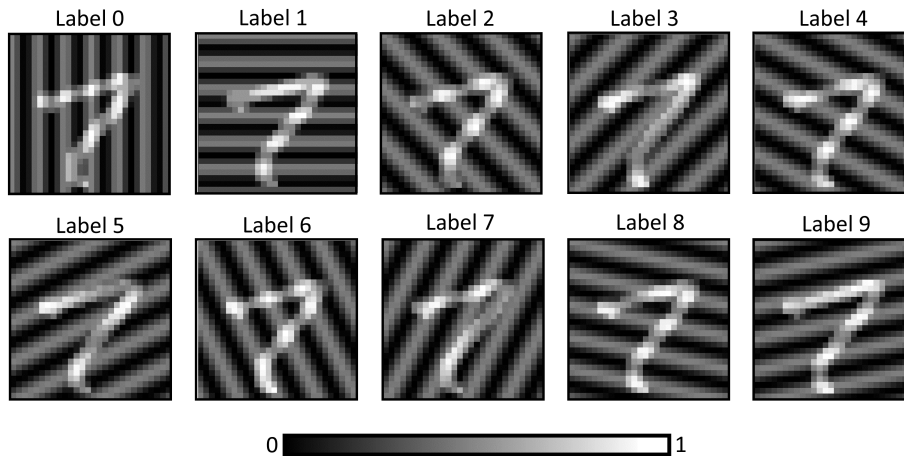


Figure 7: **Representation of the Fourier waves exploited for the spatially-extended image labelling (Set 2).** The 10 different labels, which correspond to the numbers from 0 to 9, were superimposed to the same image. In this scenario, only the Label 7 can be part of the positive dataset, while one of the other images is randomly selected to create the negative dataset

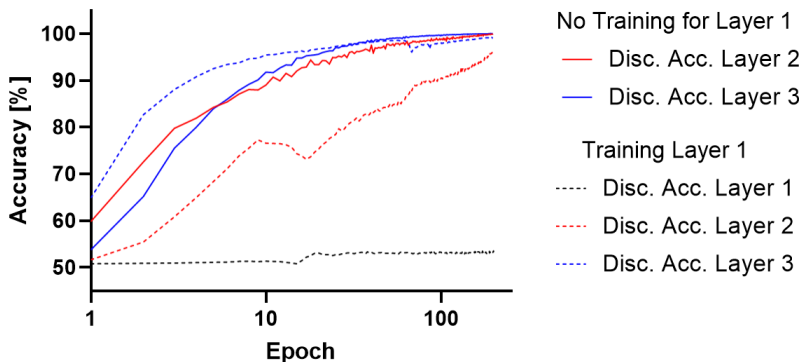


Figure 8: **Our implementation of FF-trained CNNs does not require the training of the first layer.** Continuous lines represent the accuracy values related to the classification between positive and negative dataset of the image exploited during the training phase, when the first layer is not trained. Dashed lines represent the accuracy values related to the classification between positive and negative dataset of the image exploited during the training phase, when the first layer is considered.

### Appendix C. Effect of Max Pooling on FF-trained CNNs

We also examined how max pooling layers influence FF-trained CNNs. Specifically, we tested five different configurations. Among these, two exhibited an increase in architectural complexity, characterized by a higher number of filters, which are commonly proposed for MNIST dataset analysis via CNNs. Our analysis, shown in **Table 2**, indicated a slight decrease in accuracy values when max pooling layers were applied, suggesting that preserving the entire information is preferable. Based on these results, if the conservation of computational resources is a priority, max pooling could be a viable strategy to pursue, especially for architectures with a higher number of filters, as the decrease in CNN performance is limited in such cases. However, for simpler configurations that run more quickly, max pooling significantly affects the measurements, making its application unnecessary.

<b>FF-CNN Network</b>	<b>FF Acc. [%]</b>	<b>FF + MaxPooling Acc. [%]</b>
128x128x128, filters 7x7	<b>99.14</b>	98.97
16x16x16, filters 5x5	<b>98.16</b>	97.57
64x64x64, filters 3x3	<b>98.30</b>	98.18
32x64x128, filters 7x7	<b>98.90</b>	98.54
16x32x64, filters 7x7	<b>98.47</b>	98.22

Table 2: **Max pooling layers reduce the FF-trained CNN performances.** Five FF-trained CNNs were trained and validated by using only convolutional layers or by interleaving each convolutional layer with a max pooling layer. Adam optimizer, a batch size of 50 elements and 200 epochs were considered. The classification was performed by applying the linear classifier (learning rate of  $5 \times 10^{-5}$ ). Accuracy values are characterized by an uncertainty of  $\pm 0.01$ , obtained by computing the standard deviation on the results of 5 different repetitions.

### Appendix D. Additional results CAM

For further information, refer to **Figure 9**.

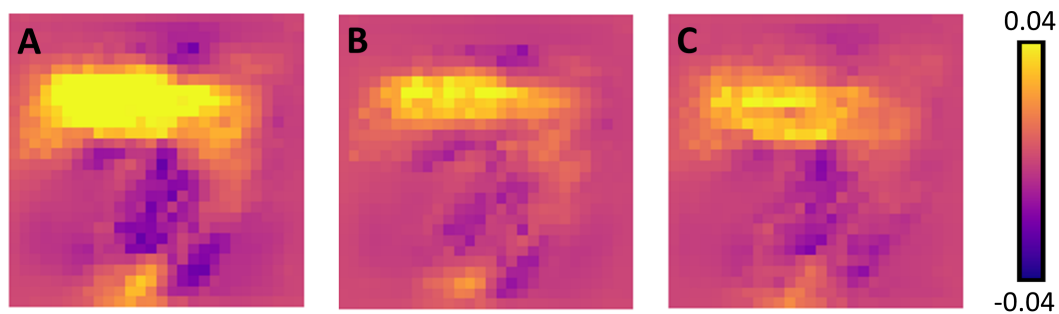


Figure 9: **Class Activation Maps show that each layer of the FF-trained CNN provides different information to the final classification outcome.** (A) shows the CAM obtained by considering both layer 2 and layer 3 of the FF-trained CNN. (B) and (C) show the CAMs obtained by independently considering the layer 2 and layer 3 of the FF-trained CNN, respectively